Random vibration testing of a quasi-zero-stiffness isolator for distribution transformers and the effects of composite damping parameters

Jiangang Ma[1], Xiaolong Wei[2], Mingxin Geng[3], Yalin Zhao[4], Liang Wang[5], Xiaochun Bai[6], Jiao Yao[7]
State Grid (Xi'an) Environmental Protection Technique Center Co., Ltd., Xi'an, China
[1]Corresponding author
E-mail: [1]*jiangang_ma@qq.com*, [2]*ya_weixiaolong@126.com*, [3]*149662969@qq.com*, [4]*15829788110@qq.com*, [5]*wangliang1889@qq.com*, [6]*13401320@qq.com*, [7]*yaojiao123@126.com*

Received 1 July 2026; accepted 15 September 2026; published online 1 November 2026
DOI https://doi.org/10.21595/vp.2026.26793

Check for updates

78th International Conference on Vibroengineering in Lviv, Ukraine, October 1, 2026

Copyright © 2026 Jiangang Ma, et al. This is an open access article distributed under the Creative Commons Attribution License, which permits unrestricted use, distribution, and reproduction in any medium, provided the original work is properly cited.

Abstract. To address low-frequency vibration and structure-borne sound transmission in distribution transformers, this study investigates a prototype quasi-zero-stiffness (QZS) low-frequency isolator with a composite particle damping unit. Broadband vertical random-vibration tests over 2-2000 Hz were conducted to evaluate the effects of particle medium and filling ratio, while a simplified nonlinear dynamic model was used to qualitatively assess the influences of structural stiffness, equivalent damping, initial oblique-spring angle, and excitation amplitude. Rubber particles, quartz sand, and hybrid particles were tested at 30 % and 60 % filling ratios using acceleration PSD ratio and isolation efficiency as the main indices. The transmission values reported in the tables are acceleration PSD ratios rather than amplitude transmissibility. Both particle medium and filling ratio significantly affect the frequency-domain response. Across the six conditions, the isolation efficiency ranges from 10.07 to 31.21 dB at 100 Hz and from 16.34 to 40.73 dB at 200 Hz. Quartz sand at 60 % filling performs best, reaching 31.21 dB and 40.73 dB, respectively. Quartz sand and hybrid particles generally show better performance at 60 % filling, whereas rubber particles show reduced performance. These results provide a reference for composite damping design and particle-medium selection in QZS isolators for distribution transformers.

Keywords: quasi-zero-stiffness isolator, particle damping, random vibration.

1. Introduction

Distribution transformers installed in noise-sensitive environments can transmit vibration through foundations and building structures, with the 100 Hz twice-line-frequency component and its 200 Hz harmonic being key targets for vibration control [1,6]. Conventional rubber and linear-spring isolators are limited by the trade-off between load-bearing stiffness and low-frequency isolation and may amplify response near resonance [1]. Quasi-zero-stiffness (QZS) isolators alleviate this conflict by combining positive- and negative-stiffness elements to achieve low dynamic stiffness near equilibrium while retaining load capacity [8], although experimental validation under realistic random vibration remains limited [3, 5]. Accordingly, this study combines simplified dynamic modeling with prototype random-vibration testing to evaluate a particle-damped QZS isolator under different structural parameters, particle media, and filling ratios. The main contribution is to link the effects of QZS structural parameters and particle-filling conditions with broadband isolation performance, providing an engineering-oriented basis for parameter comparison and damping-medium selection.

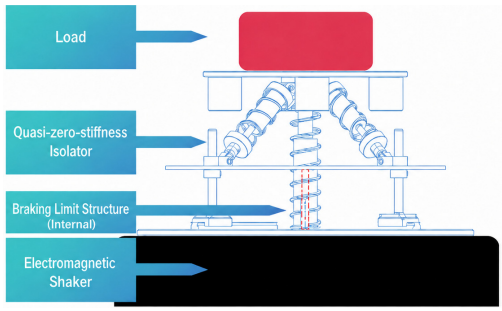
2. Design of a nonlinear isolator incorporating particle-impact damping

The proposed QZS isolator combines geometric negative stiffness with particle damping to achieve low dynamic stiffness and enhanced energy dissipation under random excitation [2, 4, 5].

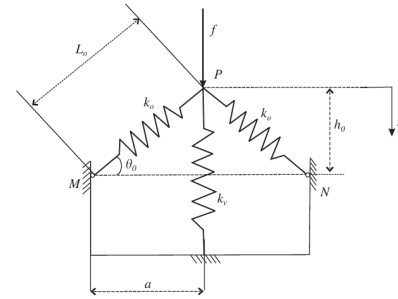
2.1. Stiffness

The QZS isolator combines a vertical positive-stiffness spring with a symmetric umbrella-linkage-oblique-spring negative-stiffness mechanism. Vertical motion of the upper plate drives radial slider motion, continuously changing the length and inclination of the pre-compressed oblique springs and generating nonlinear negative stiffness. Slider guides and mechanical limits constrain the motion and improve stability.

For the equivalent three-spring model in Fig. 1(b), k_o and L_0 denote the stiffness and initial length of each oblique spring, k_v the vertical-spring stiffness, a the horizontal half-span, h_0 the initial vertical height, θ_0 the initial oblique-spring angle, and x the downward displacement. The corresponding prototype configuration is shown in Fig. 1(a).



a) Prototype umbrella-type configuration



b) Equivalent three-spring model

Fig. 1. Structural configuration and equivalent mechanical model of the QZS isolator

The geometry gives:

$$L_0 = \sqrt{h_0^2 + a^2}, \qquad L(x) = \sqrt{(h_0 - x)^2 + a^2}, \qquad \sin\theta = \frac{h_0 - x}{L(x)}. \tag{1}$$

The nonlinear vertical restoring force generated by the two oblique springs is:

$$F_n(x) = 2k_o(h_0 - x)\left[\frac{\sqrt{h_0^2 + a^2}}{\sqrt{(h_0 - x)^2 + a^2}} - 1\right]. \tag{2}$$

Eq. (2) shows that the vertical restoring-force component decreases as the oblique springs approach the horizontal configuration, producing the required negative-stiffness effect.

The positive and total restoring forces are:

$$F_p(x) = k_v x, \tag{3}$$

$$F(x) = F_p(x) + F_n(x). \tag{4}$$

Introducing the nondimensional geometric and stiffness parameters:

$$\hat{x} = \frac{x}{L_0}, \qquad \gamma = \frac{a}{L_0} = \cos\theta_0, \qquad \alpha = \frac{k_o}{k_v}, \qquad \hat{F} = \frac{F}{k_v L_0}, \tag{5}$$

ISSN PRINT 2345-0533, ISSN ONLINE 2538-8479

the nondimensional restoring force and equivalent stiffness become:

$$\hat{F} = \hat{x} + 2\alpha\left(\sqrt{1-\gamma^2} - \hat{x}\right)\left\{\left[\hat{x}^2 - 2\sqrt{1-\gamma^2}\,\hat{x} + 1\right]^{-1/2} - 1\right\}, \tag{6}$$

$$\hat{K} = \frac{d\hat{F}}{d\hat{x}} = 1 + 2\alpha\left[1 - \frac{\gamma^2}{\left(\hat{x}^2 - 2\sqrt{1-\gamma^2}\,\hat{x} + 1\right)^{3/2}}\right]. \tag{7}$$

At the static equilibrium position, where the oblique springs are horizontal, imposing zero equivalent stiffness gives the explicit QZS matching condition:

$$\hat{x}_e = \sqrt{1-\gamma^2}, \qquad \gamma_{QZS} = \frac{2\alpha}{2\alpha+1}, \qquad \alpha_{QZS} = \frac{\gamma}{2(1-\gamma)}. \tag{8}$$

Eq. (8) provides the explicit QZS matching relation between geometry and spring stiffness [9]. The prototype analysis indicates a practical initial-angle range of approximately 37°-66° ($\gamma \approx 0.4$-0.8). Parameters are selected to satisfy Eq. (8) while maintaining positive equivalent stiffness away from equilibrium, thereby achieving low dynamic stiffness without compromising static stability [3, 4, 6].

2.2. Dynamic model

Using the nonlinear restoring force in Section 2.1, the vertical motion under base excitation is modeled as a nonlinear SDOF system with relative displacement $z(t) = u(t) - y(t)$:

$$m\ddot{z} + c\dot{z} + F(z) = -m\ddot{y}, \tag{9}$$

where m is the supported mass, c is the equivalent viscous damping, and $F(z)$ is the nonlinear restoring force. Near equilibrium, $F(z)$ is approximated by a cubic polynomial [10]:

$$F(z) \approx k_1 z + k_3 z^3, \tag{10}$$

giving the Duffing-type equation:

$$m\ddot{z} + c\dot{z} + k_1 z + k_3 z^3 = -m\ddot{y}. \tag{11}$$

For harmonic base excitation $y = Y\cos(\omega t)$, first-order harmonic balance gives:

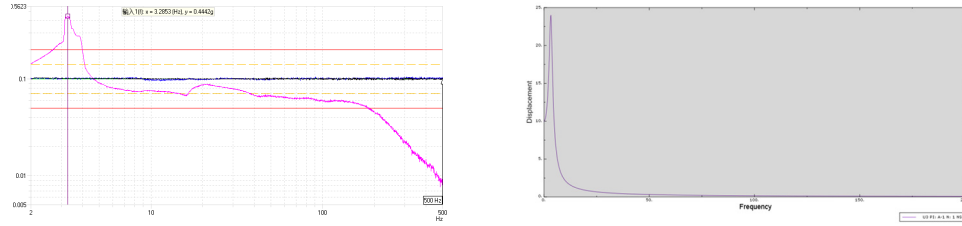
$$A^2\left[\left(k_1 + \frac{3}{4}k_3 A^2 - m\omega^2\right)^2 + (c\omega)^2\right] = (m\omega^2 Y)^2, \tag{12}$$

$$F_N = k_c\delta_n + c_c\dot{\delta}_n. \tag{13}$$

To account for particle-impact damping, a simplified particle–wall normal-contact model is adopted, in which the collision process is represented by the equivalent contact stiffness k_c and damping coefficient c_c, and the contact force in Eq. (13) is incorporated into the system dynamic equation. In this study, k_c and c_c are treated as empirical equivalent coefficients rather than parameters identified from dedicated contact experiments; therefore, the model is mainly intended to capture qualitative response trends and parameter influences rather than accurately predict absolute vibration amplitudes. The simplified model predicts a dominant low-frequency response around 3 Hz, consistent with the experimentally identified resonance region [7, 12-15].

As shown in Fig. 2, the measured natural frequency of the prototype is 3.2853 Hz, while the finite-element simulation gives 3.27882 Hz, corresponding to a relative difference of

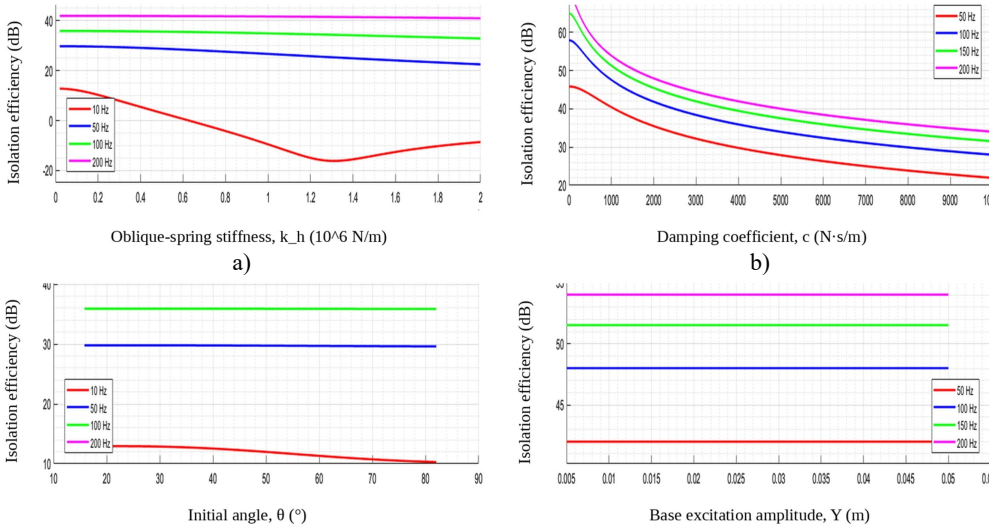
approximately 0.20 %. The two results are in good agreement, indicating that the numerical model reasonably captures the low-frequency resonance characteristics of the QZS isolator [8, 11]. The measured and simulated responses also show consistent overall trends, with a pronounced low-frequency response below about 10 Hz and effective attenuation above 20 Hz. Since the low-level sine pre-sweep was intended mainly for resonance identification rather than acquisition of a complete transmissibility curve, the available data are insufficient for reliable point-by-point curve fitting or half-power bandwidth identification. Therefore, the present model-test correlation is limited to resonance-location verification and qualitative trend assessment rather than accurate amplitude prediction.



a) b)

Fig. 2. Low-frequency model–test comparison: a) measured sine-sweep response of the prototype; b) finite-element simulated response

To further assess the engineering applicability of the simplified dynamic model, parametric simulations were carried out by independently varying the oblique-spring stiffness, system equivalent viscous damping coefficient c, initial oblique-spring angle, and base excitation amplitude while keeping the remaining parameters unchanged, as shown in Fig. 3.



a) b)

c) d)

Fig. 3. Parametric simulation results obtained from the simplified dynamic model: a) effect of oblique-spring stiffness; b) effect of equivalent damping coefficient; c) effect of initial oblique-spring angle; and d) effect of base excitation amplitude on isolation efficiency

The results indicate that increasing the oblique-spring stiffness generally reduces the isolation efficiency, demonstrating the importance of stiffness matching in maintaining the low dynamic stiffness of the QZS system. Increasing the equivalent damping coefficient suppresses the resonance response but decreases the calculated isolation efficiency in the post-resonance isolation

ISSN PRINT 2345-0533, ISSN ONLINE 2538-8479

region, indicating a trade-off between resonance control and broadband isolation. The initial angle modifies the geometric negative-stiffness contribution and thus affects the isolation efficiency, with the lower-frequency response showing greater sensitivity. In contrast, the isolation efficiency remains nearly unchanged over the investigated excitation-amplitude range, although the absolute displacement increases with excitation level. These results show that the simplified model can capture the principal effects of stiffness, damping, geometry, and excitation level on isolation performance and can therefore be used for engineering-oriented parameter comparison and qualitative trend assessment.

3. Test object, measurement system, and evaluation method

3.1. Test object and test conditions

The test object was a scaled QZS low-frequency isolator prototype for distribution transformers, tested in the vertical Z direction. Rubber particles, quartz sand, and hybrid particles were evaluated at filling ratios of 30 % and 60 %, giving six conditions under identical installation, excitation, and acquisition settings. Broadband random excitation of 2-2000 Hz with a target RMS acceleration of 0.3 g was applied. The analysis focused on the representative transformer frequencies of 100 Hz and 200 Hz, with additional data extracted at 10 Hz, 500 Hz, 1000 Hz, and 2000 Hz for broadband performance evaluation. Additional excitation-amplitude tests were also conducted to qualitatively examine the structural stability of the prototype; these tests were used for supplementary durability assessment rather than the quantitative comparison in Tables 1-3.



a) b)

Fig. 4. Experimental photographs: a) test setup; b) quartz-sand 60 % filling condition. Photos by Lian Jie in Xi'an, China, on June 18, 2026.

3.2. Measurement system and sensor arrangement

The measurement system comprised an electromagnetic shaker, dynamic data-acquisition system, accelerometers, a laser displacement sensor, fixtures, and a counterweight. Input acceleration was measured on the shaker table and output acceleration on the isolator top/counterweight, while the laser sensor monitored vertical displacement. Sensors, channels, and connections were checked and calibrated before each test.

3.3. Test procedure and evaluation method

After a low-level sine pre-sweep for resonance identification and mechanical inspection, broadband random-vibration tests were conducted for all particle-filling conditions. Input and output accelerations were synchronously recorded after the excitation reached the target level. Frequency-domain evaluation focused on 100 and 200 Hz, with 10, 500, 1000, and 2000 Hz used for broadband assessment.

For random vibration, the responses were processed as acceleration power spectral density

(PSD). Let $G_{in}(f)$ and $G_{out}(f)$ denote the input and output PSDs; the reported PSD-based vibration transmission ratio is:

$$T_{PSD}(f) = \frac{G_{out}(f)}{G_{in}(f)}. \tag{14}$$

The conventional acceleration-amplitude transmissibility is:

$$T_a(f) = \frac{A_{out}(f)}{A_{in}(f)}. \tag{15}$$

Since PSD is proportional to the squared signal amplitude, the two quantities satisfy:

$$T_a(f) = \sqrt{\frac{G_{out}(f)}{G_{in}(f)}} = \sqrt{T_{PSD}}(f). \tag{16}$$

The isolation efficiency in decibels is:

$$\eta(f) = -10\log_{10}T_{PSD}(f) = -20\log_{10}T_a(f). \tag{17}$$

Thus, $-10\log10[T_{PSD}(f)]$ and $-20\log10[T_a(f)]$ are equivalent. Table 3 therefore retains the directly processed PSD ratios, identified as acceleration PSD ratios, while $T_a(f)$ denotes the corresponding amplitude-based transmissibility; $T_{PSD}(f) < 1$ indicates spectral attenuation.

4. Random vibration test results

4.1. Consistency of random vibration input

All six conditions were tested at the same target RMS acceleration of 0.3 g and identical acquisition settings. The controlled acceleration ranged from 0.2987 to 0.3006 g, with a maximum deviation of 0.0013 g, confirming good input consistency. Although the 60 % filling conditions generally required lower drive voltages, isolation performance was evaluated from the output response, acceleration PSD ratio, and vibration attenuation rather than the drive voltage [6].

Table 1. Input consistency in the random vibration tests

Condition	Target / g	Controlled / g	Deviation / %	Drive / V
Rubber 30 %	0.3000	0.2987	−0.43	0.0252
Rubber 60 %	0.3000	0.3000	+0.00	0.0223
Quartz sand 30 %	0.3000	0.3006	+0.20	0.0245
Quartz sand 60 %	0.3000	0.2998	−0.07	0.0218
Hybrid 30 %	0.3000	0.2997	−0.10	0.0238
Hybrid 60 %	0.3000	0.3004	+0.13	0.0212

4.2. Representative-frequency data and low-frequency response

Tables 2 and 3 summarize the isolation efficiency and acceleration PSD ratio at 10-2000 Hz. At 100 and 200 Hz, the six conditions achieved isolation efficiencies of 10.07-31.21 dB and 16.34-40.73 dB, respectively. Quartz sand at 60 % filling showed the best performance, with PSD ratios of 0.000756 and 0.000085 and corresponding isolation efficiencies of 31.21 and 40.73 dB. Quartz-sand and hybrid 60 % conditions outperformed their 30 % counterparts, whereas rubber 60 % performed relatively weakly. The 10 Hz results also indicate strong sensitivity to particle medium and filling ratio, and denser low-frequency measurements remain necessary for further

evaluation near resonance.

Table 2. Summary of isolation efficiency under each condition

Frequency / Hz	Rubber 30 %	Rubber 60 %	Quartz sand 30 %	Quartz sand 60 %	Hybrid 30 %	Hybrid 60 %
10	1.57	0.47	2.34	11.44	1.03	2.07
100	18.21	10.07	19.75	31.21	16.24	20.57
200	25.28	16.34	27.02	40.73	23.51	26.68
500	33.82	27.40	36.01	46.13	33.41	34.77
1000	33.84	32.32	36.77	45.34	34.42	35.79
2000	29.65	32.36	29.65	32.76	24.70	27.47

Table 3. Summary of acceleration PSD ratio under each condition

Frequency / Hz	Rubber 30 %	Rubber 60 %	Quartz sand 30 %	Quartz sand 60 %	Hybrid 30 %	Hybrid 60 %
10	0.696354	0.897076	0.582823	0.071832	0.789256	0.621540
100	0.015106	0.098493	0.010605	0.000756	0.023783	0.008779
200	0.002963	0.022727	0.001988	0.000085	0.004462	0.002149
500	0.000415	0.001820	0.000251	0.000024	0.000456	0.000334
1000	0.000413	0.000586	0.000210	0.000029	0.000361	0.000264
2000	0.001085	0.000580	0.001085	0.000530	0.003389	0.001792

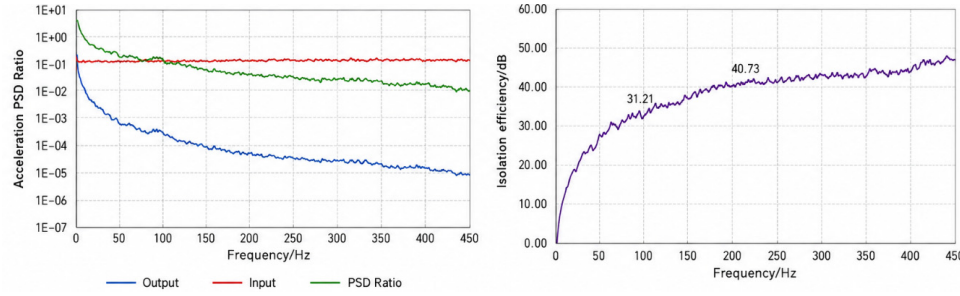


Fig. 5. PSD ratio and isolation efficiency for quartz sand at 60 % filling

5. Discussion on the effects of composite damping parameters

Both particle medium and filling ratio significantly affect the isolation performance of the QZS isolator. During the experiments, multiple test conditions were implemented by repeatedly changing the particle medium and filling state, including rubber particles, quartz sand, and hybrid particles at filling ratios of 30 % and 60 %. At 30 % filling, quartz sand performed slightly better than rubber and hybrid particles; at 60 % filling, its advantage became more pronounced, with isolation efficiencies of 31.21 dB and 40.73 dB at 100 Hz and 200 Hz, respectively, which may be attributed to stronger frictional and collisional energy dissipation. Increasing the filling ratio from 30 % to 60 % improved the performance of quartz sand and hybrid particles at these frequencies but reduced that of rubber particles. A possible explanation is that, at a higher rubber-particle filling ratio, the available free space for particle motion is reduced, which may promote particle stacking and constrain relative motion, thereby decreasing effective particle-wall and particle–particle collisions and weakening the associated energy dissipation [12-14]. Since particle motion and collision frequency were not measured directly in the present experiments, this interpretation is regarded as a plausible mechanism rather than a quantitatively verified conclusion. Therefore, the filling ratio should be selected according to the particle medium and target frequency band. In addition, continuous broadband random-vibration durability tests and supplementary tests under different excitation amplitudes were conducted. No obvious loosening, deformation, abnormal collision, or structural damage was observed during repeated condition

changes and sustained vibration, and the major components remained intact after testing, indicating satisfactory short-term structural stability and adaptability under the present test conditions. However, the current experiments were mainly conducted under normal laboratory conditions; dedicated high- and low-temperature tests, humidity-aging tests, and longer-term cyclic-fatigue evaluations are still required to comprehensively assess the engineering applicability of the isolator.

6. Conclusions

A scaled QZS low-frequency isolator for distribution transformers was evaluated by sine pre-sweep and broadband random-vibration tests. The prototype exhibited a low-frequency resonance near 3.3 Hz, while the six particle-filling conditions showed clear performance differences at 100 and 200 Hz. Quartz sand at 60 % filling provided the best isolation, achieving 31.21 dB and 40.73 dB at the two representative frequencies. Both particle medium and filling ratio significantly influenced the response, and a higher filling ratio did not always improve performance, as demonstrated by the reduced effectiveness of rubber particles at 60 % filling. The results indicate that particle medium and filling ratio should be selected according to the target frequency band, while further low-frequency measurements are required for more detailed resonance-region evaluation.

Acknowledgements

This work was supported by the Science and Technology Project of State Grid (Xi'an) Environmental Protection Technology Center Co., Ltd., "Development of a Quasi-Zero-Stiffness Low-Frequency Isolator for Distribution Transformers".

Data availability

The datasets generated during and/or analyzed during the current study are available from the corresponding author on reasonable request.

Conflict of interest

The authors declare that they have no conflict of interest.

References

[1] Q. Fang, Z. Ye, and C. Chen, "A review of power transformer vibration and noise caused by silicon steel magnetostriction," *Electronics*, Vol. 13, No. 5, p. 968, Mar. 2024, https://doi.org/10.3390/electronics13050968

[2] Q. Liu, Z. Li, J. Wang, J. Lian, and Y. Wang, "Research progress on quasi-zero-stiffness low-frequency vibration isolation technology," (in Chinese), *Journal of Mechanical Strength*, Vol. 43, No. 1, pp. 17–26, 2021, https://doi.org/10.16579/j.issn.1001.9669.2021.01.003

[3] B. Yan, N. Yu, and C. Wu, "A state-of-the-art review on low-frequency nonlinear vibration isolation with electromagnetic mechanisms," *Applied Mathematics and Mechanics*, Vol. 43, No. 7, pp. 1045–1062, 2022, https://doi.org/10.1007/s10483-022-2868-5

[4] G. Sui, X. Zhang, S. Hou, X. Shan, W. Hou, and J. Li, "Quasi-zero stiffness isolator suitable for low-frequency vibration," *Machines*, Vol. 11, No. 5, p. 512, Apr. 2023, https://doi.org/10.3390/machines11050512

[5] H. Ye, Y. Wang, B. Liu, and X. Jiang, "Experimental study on the damping effect of multi-unit particle dampers applied to bracket structure," *Applied Sciences*, Vol. 9, No. 14, p. 2912, Jul. 2019, https://doi.org/10.3390/app9142912

[6] A. D. Shaw, S. A. Neild, and D. J. Wagg, "Dynamic analysis of high static low dynamic stiffness vibration isolation mounts," *Journal of Sound and Vibration*, Vol. 332, No. 6, pp. 1437–1455, Dec. 2012, https://doi.org/10.1016/j.jsv.2012.10.036

[7] X. Wang, Y. Shan, X. Liu, T. He, and J. Wu, "Comparison of the vibration reduction effects of particle dampers under swept-sine and random excitations," (in Chinese), *Noise and Vibration Control*, No. 5, p. 198, 2014, https://doi.org/10.3969/j.issn.1006-1335.2014.05.043

[8] C. Liu, W. Zhang, K. Yu, T. Liu, and Y. Zheng, "Quasi-zero-stiffness vibration isolation: designs, improvements and applications," *Engineering Structures*, Vol. 301, p. 117282, Dec. 2023, https://doi.org/10.1016/j.engstruct.2023.117282

[9] Z.-Q. Zhang, M.-Q. Niu, and L.-Q. Chen, "Analysis and optimization of a quasi-zero-stiffness vibration isolator based on partially rigidized compliant mechanisms," *Engineering Structures*, Vol. 343, p. 121048, Aug. 2025, https://doi.org/10.1016/j.engstruct.2025.121048

[10] N. A. Saeed, L. Hou, H. Yi, A. A. Shukur, S. M. Alamry, and S. M. El-Shourbagy, "On a broadband vibration isolator with tunable stiffness: from quasi-zero-stiffness to zero-stiffness behavior," *Applied Mathematics and Mechanics*, Vol. 47, No. 2, pp. 255–282, 2026, https://doi.org/10.1007/s10483-026-3351-9

[11] N. Y. P. Vo, T. D. Le, and M. K. Nguyen, "A quasi-zero stiffness-based low-frequency vibration isolation platform: experimental investigation," *Machines*, Vol. 14, No. 5, p. 546, May 2026, https://doi.org/10.3390/machines14050546

[12] Y. Zhu, X. Guo, Q. Wang, and D. Cao, "A lightweight tuned particle damper for low-frequency vibration attenuation," *Journal of Sound and Vibration*, Vol. 583, p. 118440, Apr. 2024, https://doi.org/10.1016/j.jsv.2024.118440

[13] B. B. Prasad, F. Duvigneau, T. Reinboth, D. Juhre, and E. Woschke, "Design strategies of particle dampers for large-scale applications," *Journal of Vibration Engineering and Technologies*, Vol. 12, No. 4, pp. 5715–5746, 2023, https://doi.org/10.1007/s42417-023-01214-x

[14] Y. Zhu, X. Guo, and D. Cao, "Research progress on tuned particle dampers: a review of modeling, energy dissipation mechanisms, and applications," *European Journal of Mechanics – A/Solids*, Vol. 113, p. 105720, May 2025, https://doi.org/10.1016/j.euromechsol.2025.105720

[15] K. Yang et al., "Mode-resolved, reconfigurable particle damping for printed circuit boards vibration control," *Mechanical Systems and Signal Processing*, Vol. 248, p. 113995, Feb. 2026, https://doi.org/10.1016/j.ymssp.2026.113995